

Article

# Machinability of Eco-Friendly Lead-Free Brass Alloys: Cutting-Force and Surface-Roughness Optimization

Anagnostis I. Toulfatzis <sup>1,2</sup>, George A. Pantazopoulos <sup>1,\*</sup> , Constantine N. David <sup>3</sup>,  
Dimitrios S. Sagris <sup>3</sup>  and Alkiviadis S. Paipetis <sup>2,\*</sup>

<sup>1</sup> ELKEME Hellenic Research Centre for Metals S.A., 56th km Athens—Lamia National Road, 32011 Oinofyta, Greece; atoulfatzis@elkeme.vionet.gr

<sup>2</sup> Department of Materials Science and Engineering, University of Ioannina, 45110 Ioannina, Greece

<sup>3</sup> Department of Mechanical Engineering, Technological Education Institute of Central Macedonia, 62124 Serres, Greece; david@teicm.gr (C.N.D.); dsagris@teicm.gr (D.S.S.)

\* Correspondence: gpantaz@elkeme.vionet.gr (G.A.P.); paipetis@cc.uoi.gr (A.S.P.);  
Tel.: +30-2262-60-4463 (G.A.P.); +30-265-100-8001 (A.S.P.)

Received: 22 March 2018; Accepted: 4 April 2018; Published: 8 April 2018



**Abstract:** The machinability in turning mode of three lead-free brass alloys, CuZn42 (CW510L), CuZn38As (CW511L) and CuZn36 (C27450) was evaluated in comparison with a reference free-cutting leaded brass CuZn39Pb3 (CW614N), as far as the quality characteristics, i.e., cutting force and surface roughness, were concerned. A design of experiments (DOE) technique, according to the Taguchi L<sub>16</sub> orthogonal array (OA) methodology, as well as analysis of variance (ANOVA) were employed in order to identify the critical-to-machinability parameters and to obtain their optimum values for high-performance machining. The experimental design consisted of four factors (cutting speed, depth of cut, feed rate and alloy) with four levels for each factor using the “smaller-the-better” criterion for quality characteristics’ optimization. The data means and signal-to-noise (S/N) responses indicated that the depth of cut and the feed rate were the most influential factors for the cutting force and surface roughness, respectively. The optimized machining parameters for cutting force (34.59 N) and surface roughness (1.22 μm) minimization were determined. Confirmation experiments (cutting force: 39.37 N and surface roughness: 1.71 μm) seem to show that they are in close agreement to the main conclusions, thereby validating the findings of the statistical evaluation performed.

**Keywords:** cutting force; surface roughness; lead-free brasses; turning; machinability; design of experiments (DOE)

## 1. Introduction

Brass alloys, one of the most important classes of copper alloys, are widely used for many mechanical and industrial applications such as mechanical, electrical and hydraulic systems [1]. Brasses exhibit a beneficial combination of low cost, improved machinability, corrosion resistance and good formability [2]. The fabrication of the final brass component, i.e., in a turning operation, is facilitated significantly by the lead (Pb) that exists in leaded-brass alloys [3]. In recent years, the dangerous effects of lead upon human health and the environment, stricter regulations for allowable lead content levels in products, have encouraged the development of lead-free brass alloys [4]. However, the absence of lead from the brass alloys deteriorates the machining quality due to the fact that lead acts as a lubricant and chip-breaking component [5]. Understanding the material behaviour in lead-free brass alloys concerning chip fracture and formation mechanisms is vital in order to design candidate alloys for the substitution of conventional leaded brasses without compromising the reliability and performance of manufactured components [6]. Due to recent regulations that encourage

the promotion of new lead-free brasses, scientific research concerning the study and the development of special machinable brasses concerning machinability performance and optimization has become very challenging and important. The development of a suitable grain and phase structure (the presence of  $\alpha$ ,  $\beta$  or  $\gamma$  phases in Cu-Zn system), through various metallurgical methods, e.g., alloying, forming, heat treating, etc. exerts a major influence on fracture behaviour and, consequently, on chip-breaking properties and machinability performance [7–10].

The effect of alloy additives, such as graphite and bismuth, was investigated concerning the machinability and mechanical properties of lead-free brass alloys. A lead-free machinable brass (CuZn40) exhibiting good balance between the elongation and the machinability was obtained by using the mixed powder containing 0.5 wt % graphite particles and 2.2 wt % Bi additions [11]. Relevant research revealed the benefits of the recycled bismuth-tin solder addition in lead-free brass alloy (Cu-38Zn-0.5Si) by reducing the chip-size morphology as well as the required cutting force [12]. The improvement of chip-breaking efficiency was attributed to the presence of  $\kappa$ -phase in CuZn21Si3P, as opposed to the effect of  $\alpha$ -phase in CuZn38As brass. Likewise, the high percentage of  $\beta$ -phase in the microstructure of CuZn41.5 resulted in the reduction of chip morphology and cutting forces [13]. Heat treatments were also performed in lead-free brass alloys (CuZn42, CuZn38As and CuZn36) in order to modify the microstructure and increase the  $\beta$ -phase content providing a promising ground for better chip breakability and improved machinability [14]. The influence of the coating type (TiN, TiAlN, TiB<sub>2</sub> and DLC on carbide tools) as well as the use of polycrystalline diamond (PCD) tools on machining forces, chip formation and workpiece quality, was analyzed for the evaluation of machinability in three low-lead brass alloys (CuZn38As, CuZn42, and CuZn21Si3P). The machining problems were diminished using a diamond-like carbon coating, especially by the reduction of the friction in the secondary shear zone [15]. A machinability comparison between leaded (CuZn39Pb3) and lead-free brass (CuZn21Si3P) alloys was implemented in a relevant work concerning tool wear during machining. Machining of the lead-free brass alloy (CuZn21Si3P) resulted in higher cutting forces, longer chip size and, eventually, higher tool-wear rates using cemented carbides. The use of coating on carbide tools (e.g., (Ti,V,Zr,Hf,Nb,Ta)N), was recommended as a possible solution for overcoming excessive tool-wear rates [16].

Surface quality is of major significance, and explicitly demanded in high-precision and productivity machining processes. Moreover, the use of high-speed cutting ensures increased productivity, workpiece dimensional accuracy and improved surface finish [17]. Cutting force is also another important machinability performance indicator, which constitutes a criterion for the selection of optimal process conditions, affecting tool lifetime significantly. Cutting forces could also be calculated using mathematical models and employing renowned machining theories (Oxley's machining theory) based on the determination of strain rates along the shear plastic zone and tool/chip interface [18,19].

Design of experiments (DOE) and genetic algorithm (GA) approaches are powerful and well-established techniques employed to investigate the optimization of cutting parameters such as cutting speed, feed rate, depth of cut, minimum quantity of lubrication (MQL), and alloy type [20–23].

Artificial neural networks (ANN) and response surface methodology (RSM) were used to determine the effect of cutting conditions (cutting speed, feed rate and depth of cut) on cutting force, surface roughness and tool wear during milling of Ti-6242S alloy [24]. In micromilling, tool wear and fracture as well as intense burr formation, and poor surface quality, are considered as the major quality problems. A relevant study investigated the effect of cutting path on the cutting force and surface quality in a micromilling process under different cooling conditions (e.g., dry, air blow, and flood-cooling agent) at fixed cutting parameters [25].

Cutting force and chip segmentation are also well reproduced using finite element method (FEM) (arbitrary Lagrangian-Eulerian and Lagrangian methods) and it was found that chip fragmentation can be correlated to the results of the cutting force development [26].

In a previous research work, the chip morphology and power consumption were employed as the major quality characteristics (criteria) for the ranking of machining performance [8]. In this work, a first effort was made to optimize two quality characteristics, cutting force and surface roughness, during turning of the studied brass alloys. The methodology used for the optimization was supported by signal-to-noise ratio data means, as dictated by the Taguchi experimental design and ANOVA. This technique is an efficient and economical way to treat and optimize industrial processes [27–29]. The present work is an original contribution, pertaining to the optimization of machinability of environmentally friendly lead-free brass alloys (CuZn42, CuZn38As and CuZn36), in comparison to a conventional leaded-brass alloy (CuZn39Pb3). The emergence of new legislation for the environment and health and safety (e.g., drinking-water regulations), together with the necessity to design and manufacture new lead-free machinable alloys, render this project as of high industrial significance. To the best of our knowledge, the present work is novel, since there is not any other published work in this specific area that provides an optimization guideline for cutting force and surface roughness during machining of these lead-free brass alloy classes. It reflects also the original experimental and statistical work performed by the authors, as a part and continuation of a long-term industrial research and development (R&D) project.

## 2. Materials and Methods

### 2.1. Experimental Design

The research approach was based on the experimental methodology applied aiming to evaluate the alloy performance in a more holistic view, which is presented schematically in the following flow chart (Figure 1).

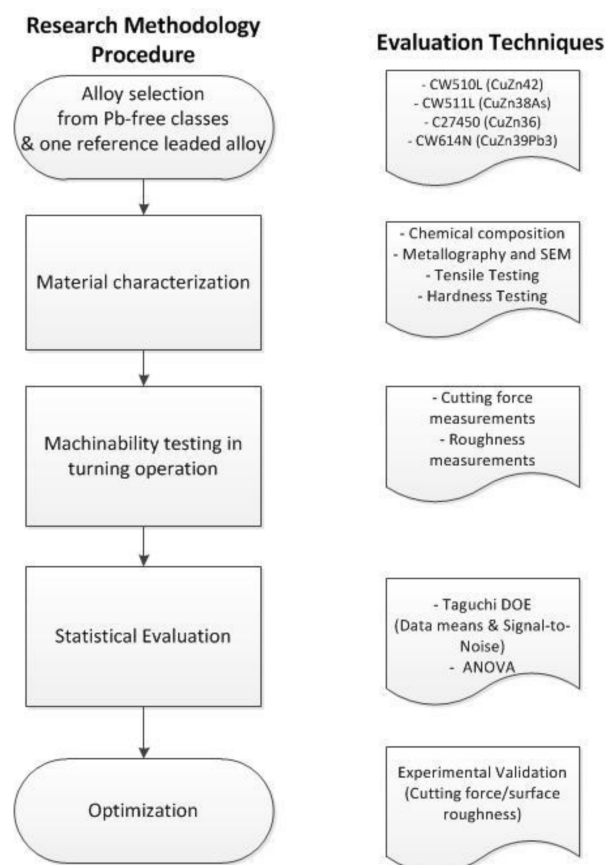


**Figure 1.** Flowchart of the experimental methodology applied for the present research.

## 2.2. Alloys and Chemical Composition

Extruded and drawn bars of 35 mm diameter and 200 mm length manufactured from three lead-free brass alloys, namely CuZn42 (CW510L), CuZn38As (CW511L) and CuZn36 (C27450), as well as a leaded brass, namely CuZn39Pb3 (CW614N), were selected for this study. The metallurgical condition of the bars was adjusted at the standard half-hard temper by the applied manufacturing process. The microstructure and mechanical properties were studied in previous research works [6,8,14], as shown in Table 1.

**Table 1.** Mechanical properties and  $\beta$ -phase percentage.

Brass Alloys	$R_{p0.2}$ (MPa)	$R_m$ (MPa)	$A_{50}$ (%)	Hardness HV1	$\beta$ -Phase (%)
CW614N	300	430	28	132	33
CW510L	250	460	41	127	60
CW511L	250	380	42	116	5
C27450	185	320	48	98	2

The composition of the alloys, as determined by optical emission spectrometry (OES) (ARL, Waltham, MA, USA) and X-ray fluorescence (XRF) (ARL, Waltham, MA, USA), is shown in Table 2. The chemical composition of the samples was compared with the EN 12164 standard and the Copper Development Association (CDA) [30].

**Table 2.** Chemical composition of the studied brass alloys (expressed in % m/m).

Alloy/(Spec. Limits)	Sn	Zn	Pb	Fe	Ni	Al	Cu
CuZn39Pb3 (CW614N)	0.26	Rem.	2.97	0.23	0.064	0.018	58.32
EN 12164 (CuZn39Pb3/CW614N)	0.30 max	Rem.	2.5–3.5	0.30 max	0.30 max	0.050 max	57–59
CuZn42 (CW510L)	0.0058	Rem.	0.10	0.0342	0.0030	0.0002	57.46
EN 12164 (CuZn42/CW510L)	0.30 max	Rem.	0.20 max	0.30 max	0.30 max	0.050 max	57–59
CuZn38As (CW511L)	0.0042	Rem.	0.09	0.0189	0.0012	0.0002	62.04
EN 12164 (CuZn38As/CW511L)	0.10 max	Rem.	0.20 max	0.10 max	0.30 max	0.050 max	61.5–63.5
CuZn36 (C27450)	0.0144	Rem.	0.21	0.0244	0.0030	0.0247	63.38
Copper Development Association (CDA) (CuZn36/C27450)	-	Rem.	0.25 max	0.35 max	-	-	60–65

## 2.3. Microstructure and Mechanical Testing

Microstructural characterization of the subject materials was conducted on transverse cross-sections after wet grinding by up to 1200 grit SiC paper followed by fine polishing using diamond and silica suspensions. Subsequently, immersion chemical etching for approximately 5 s at room temperature was performed using FeCl<sub>3</sub>-based solutions according to the ASTM E407-07 standard [31]. Quantitative optical metallography was performed using a Nikon Epiphot 300 (Nikon, Tokyo, Japan) inverted light optical microscope using image analysis software (Image Pro Plus, Rockville, MD, USA) for phase (area) fraction measurements. High-magnification observations, utilizing a FEI XL40 SFEG scanning electron microscope (FEI, Eindhoven, The Netherlands), were performed on mounted specimens using both secondary electron (SE) and back-scattered electron (BSE) signals under 20 kV accelerating voltage. Tensile tests were performed using an Instron 8802 250 kN (Instron, Norwood, MA, USA) servohydraulic testing machine at ambient temperature according to BS EN ISO 6892-1 standard [32]. Vickers hardness tests, using a diamond indenter, were performed at various locations on transverse sections (surface-midway-centre) employing an Instron Wolpert 2100 hardness tester, under 1.0 kg (9.807 N) applied load, according to BS EN ISO 6507 [33].

## 2.4. Machinability Testing

The machinability of the studied brass alloys was experimentally evaluated in terms of cutting force (CF) and surface roughness (SR) measurements. Machinability tests were performed in a turning

operation on a Computerized Numerical Control (CNC) lathe machine (DMG Alpha 500, DMG MORI CO. LTD, Tokyo, Japan) according to the instructions of ISO 3685 standard [34]. Uncoated cemented Mitsubishi carbide cutting-tool inserts, with grade name HTi10, ISO range K10 and ANSI range C3 (Figure 2a), were used to conduct the machinability tests [20]. The selected carbide grade is ideal for turning non-ferrous metals, while it ensures high rigidity and wear resistance. The machining length for each bar was 150 mm and it was kept constant throughout all the experiments. The turning process was performed without any lubrication.

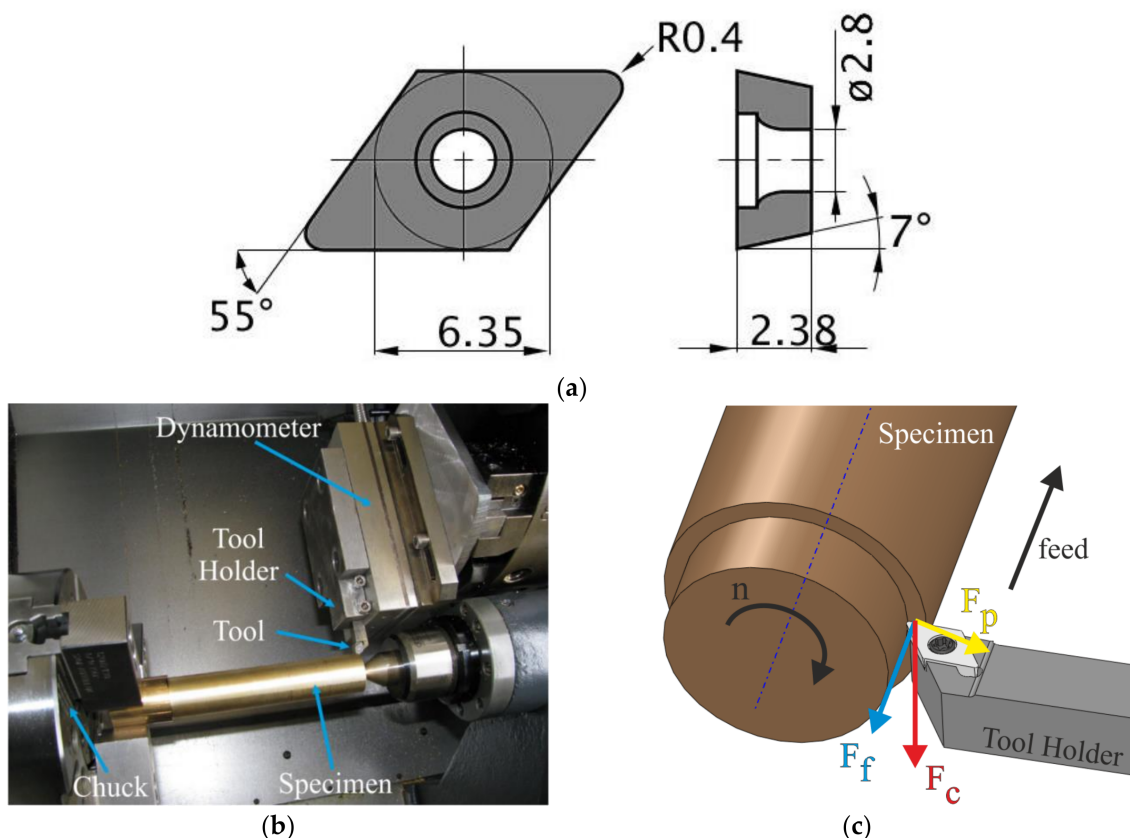


**Figure 2.** (a) Cemented carbide-cutting insert geometry (in mm) [8]; (b) set-up for the measurement of the cutting forces; and (c) machining kinematics and the cutting-force components that were measured in all experiments.

For the measurement of the cutting forces, a specific setup, as illustrated in Figure 2b, was employed. The cutting forces were acquired using a 3-axis dynamometer (Kistler 9257B) and an appropriate analog-to-digital device (NI PCI-MIO-16E—1MHz) controlled by means of a graphical user interface (GUI) code developed under LabVIEW 11 software (National Instruments, Austin, TX, USA).

Figure 2c illustrates the machining kinematics and the cutting-force components that were measured in all experiments. The three cutting-force components that arise due to the cutting process and the chip formation are the following: the main cutting force  $F_c$ , the passive force  $F_p$ , and the feed direction force  $F_f$ . The magnitude of the main cutting force was dominant in comparison to the other force components and, therefore, the machinability study was focused specifically on this force component. As shown, the main cutting force  $F_c$  is built up immediately at the entry of the cutting tool in the rotating specimen and it becomes both a static ( $F_{c, st}$ ) and dynamic part ( $F_{c, dyn}$ ), apparently.

The static part is stable throughout the whole measurement and determines the mean value of the main cutting force, which is taken into account in this study. Moreover, it expresses the

specific cutting resistance of the machined material and, therefore, is assumed as a criterion of the machinability evaluation. Regarding the emerged dynamic part of the cutting force, an amplitude distortion due to the chip formation, chip flow and chip segmentation was evident. In order to achieve reliable results, two repetitions of the turning tests were performed for each set of the selected cutting parameters and the average value of the measured main cutting force was considered in the subsequent evaluation analysis.

The surface roughness (SR) as the second criterion selected for machinability evaluation was exploited. A complete system for quantitative 3D topography including a Wyko NT1100 Optical Profiling system (Veeco, Tucson, AZ, USA) supported by Wyko Vision 32 analysis software was utilized. This provides an accurate, non-contact surface metrology based on white-light interferometry to achieve a high resolution of 3D surface roughness measurements at nanometer scale. In this study, the three-dimensional roughness average ( $R_a$ ) over the entire measured area according to ASME-ANSI B46.1 was evaluated [35]. Roughness average ( $R_a$ ) was selected as the most representative surface-roughness characteristic, used in case of industrial applications in brass component manufacturing. Although this is a partial surface-topography evaluation (other features of roughness were also retrieved, such as  $R_z$ ,  $R_t$ , etc.), it is considered the most suitable parameter for such comparison measurements since it constitutes a very common quality criterion included in relevant customer specifications.

Figure 3 illustrates the principle of 3D white-light interferometry for surface roughness measurement, which was adopted as the most adequate technique for the scope of the current research. The surface analysis results comprise the 3D topographical map and 2D cross-sections, which show both the shape and the resulting roughness. Furthermore, all tribological data according to the ASME-ANSI B46.1 standard were calculated. As mentioned above, two repetitions were also exploited for each set of the selected cutting parameters and the average roughness value was deduced.

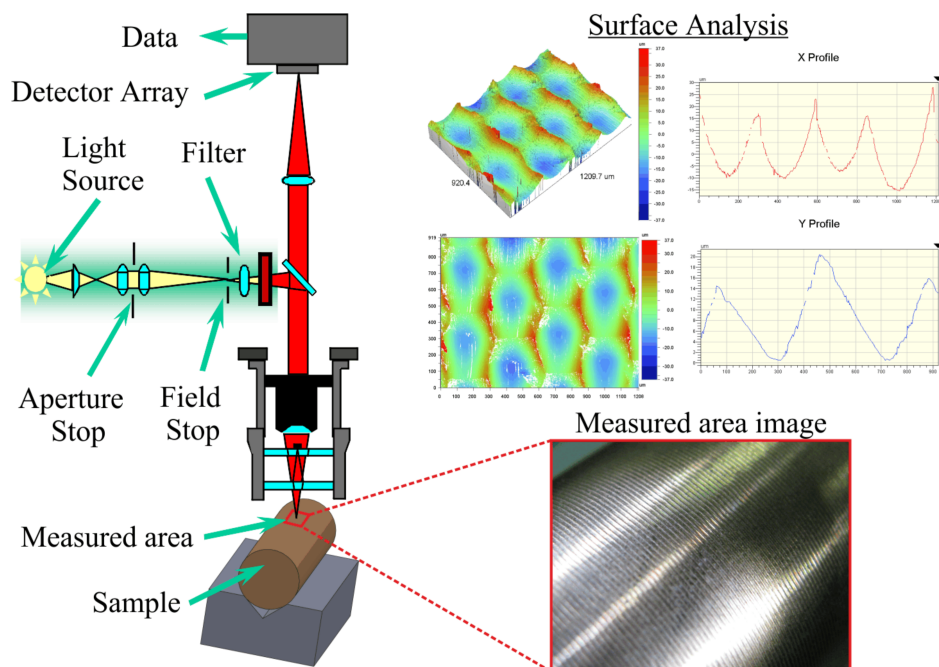


**Figure 3.** 3D white-light interferometry for surface-roughness measurement.

### 2.5. Statistical Evaluation

For the elaboration of machinability optimization, a method of Taguchi for 4 factors at 4 levels was employed. The number of levels is defined mainly by the available brass alloys for comparison (CW614N, CW510L, CW511L and C27450). The individual cutting parameters (depth of cut, feed rate

and cutting speed) for each level, were carefully selected in order to apply this methodology for the entire spectrum of machining conditions utilized on the present equipment. A design of experiments (DOE) Taguchi method and ANOVA were conducted to reduce the number of experiments using Minitab Software (version 16, Minitab Inc., State College, PA, USA). The orthogonal array approach proposed by Taguchi has been used for the experimental design. Four machining parameters, namely cutting speed (CS), depth of cut (DC), feed rate (FR) and material (M), were selected as control factors. Several preliminary experiments were executed for the determination of the ranges of the cutting conditions. Table 3 presents the process parameters and their levels. The appropriate choice for planning the experiments, according to Taguchi's quality in design concept, was the standard L<sub>16</sub> (44) orthogonal array (OA), which is shown in completed form in Table 4.

**Table 3.** Process parameters and their levels.

Parameters	Units	Level 1	Level 2	Level 3	Level 4
Cutting Speed	rpm (m/min)	1500 (165)	1750 (192)	2000 (220)	2250 (247)
Depth of Cut	mm	0.5	1.0	1.5	2.0
Feed Rate	mm/min	150	200	250	500
Material	-	CW510L	CW511L	C27450	CW614N

**Table 4.** L<sub>16</sub> standard orthogonal array for the experiments.

Number of Experiment	Parameters			
	Cutting Speed (rpm)	Depth of Cut (mm)	Feed Rate (mm/min)	Material
1	1500	0.5	150	CW510L
2	1500	1.0	200	CW511L
3	1500	1.5	250	C27450
4	1500	2.0	500	CW614N
5	1750	0.5	200	C27450
6	1750	1.0	150	CW614N
7	1750	1.5	500	CW510L
8	1750	2.0	250	CW511L
9	2000	0.5	250	CW614N
10	2000	1.0	500	C27450
11	2000	1.5	150	CW511L
12	2000	2.0	200	CW510L
13	2250	0.5	500	CW511L
14	2250	1.0	250	CW510L
15	2250	1.5	200	CW614N
16	2250	2.0	150	C27450

### 3. Results and Discussion

#### 3.1. Microstructure and Mechanical Properties

Metallographic evaluation revealed a duplex-phase microstructure consisting of a mixture of  $\alpha$ - $\beta$  phases of variable content, as anticipated in the Cu-Zn alloy system (Figures 4 and 5). Moreover, the microstructure of the CW614N alloy contains ~3% Pb particles, which appeared as black dots (in optical micrographs), that are non-dissolved in  $\alpha$ - or  $\beta$ -phase (Figure 4a). Scanning electron microscopy (SEM) observations at higher magnification ( $\times 1000$ ) confirmed the findings of the optical microscopy concerning the variation of  $\beta$ -phase content for each studied brass alloy (Figure 5).

The tensile properties augmented significantly with the increase of  $\beta$ -phase volume fraction in brass alloys. More specifically, CW510L (60%  $\beta$ -phase) and CW614N (33%  $\beta$ -phase) exhibited the highest tensile strength (460 MPa and 430 MPa, respectively) and hardness (127 HV and 132 HV, respectively), while they show the lowest total elongation (41% and 28%, respectively), compared to CW511L and C27450 alloys, see also Table 1 and Figures 4 and 5 [6]. The  $\beta$ -phase content is inherently

related to the machinability and most effectively to the chip breakability [36]. Chip breaking is mainly controlled by the distribution of Pb particles in conventional leaded brass alloys, while  $\beta$ -phase fraction exerts a major influence on shear band formation and micro-crack generation in lead-free alloys. In a previous research work, CW614N and CW510L possessed the optimum chip-breaking capability, followed by C27450 and CW511L alloys. The C27450 was marginally superior compared with CW511L alloy, due to its slightly higher content of Pb, which promotes chip breaking [8]. Apart from chip-breaking capability, additional characteristics such as cutting force and surface roughness play an important role in ranking machinability performance. The respective results, pertaining to the optimization of the aforementioned characteristics, are discussed in the following sections.

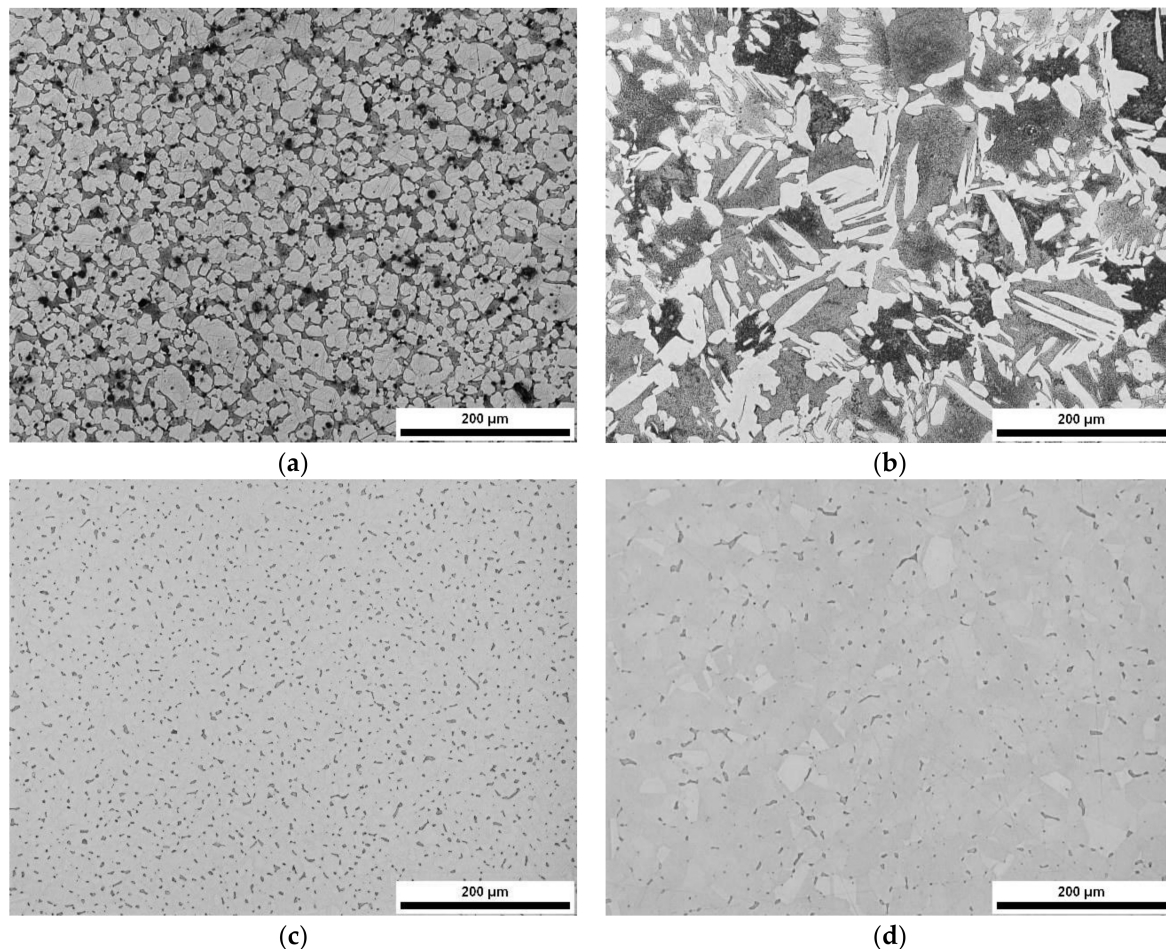


**Figure 4.** Optical micrographs of the microstructure on transverse sections: (a) CuZn39Pb3 (CW614N) leaded brass as well as (b) CuZn42 (CW510L); (c) CuZn38As (CW511L) and (d) CuZn36 (C27450) lead-free brasses. Light areas represent  $\alpha$ -phase and dark areas represent  $\beta$ -phase. In (a) there is an appreciable amount of Pb particles, which appeared as black dots.

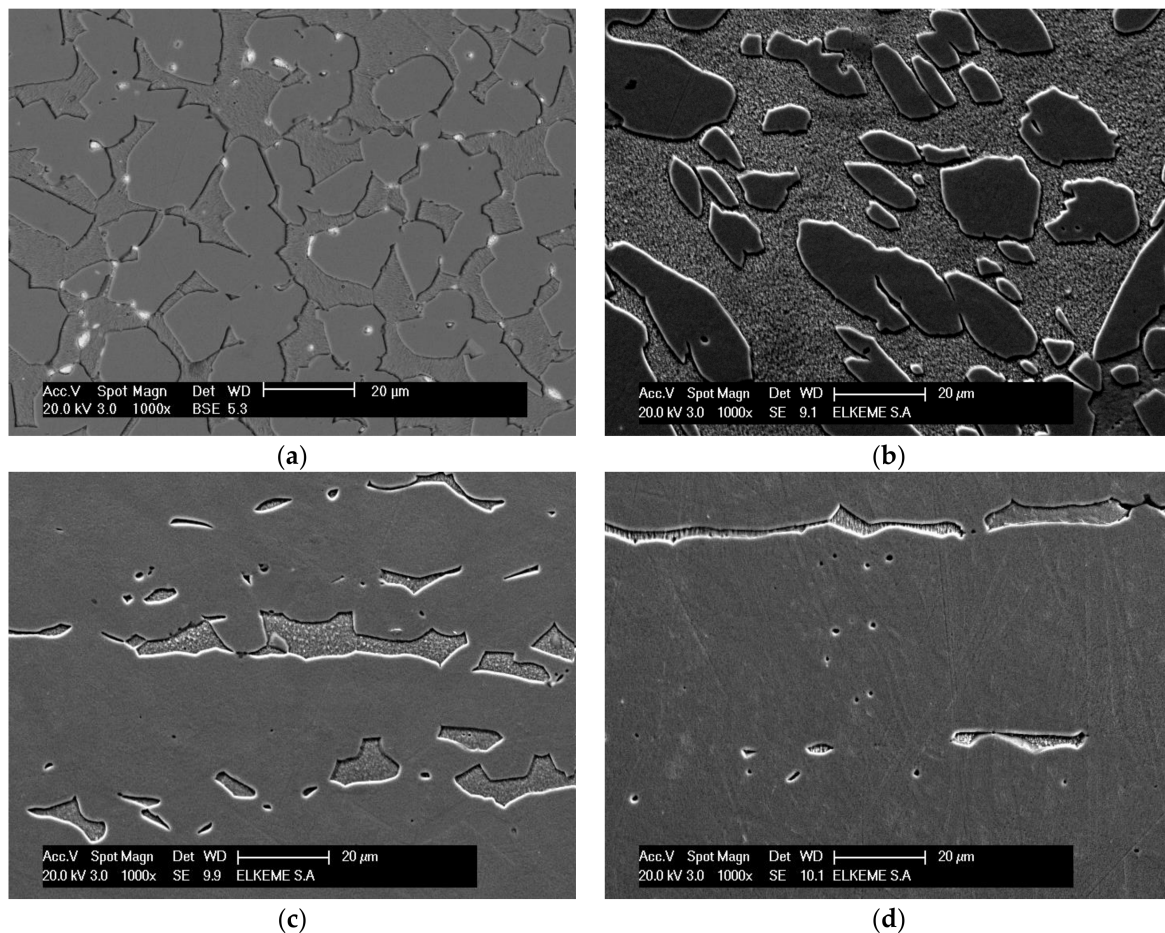


**Figure 5.** Scanning electron microscopy (SEM) micrographs under secondary and backscattered electron imaging: (a) CuZn39Pb3 (CW614N) leaded brass as well as (b) CuZn42 (CW510L); (c) CuZn38As (CW511L) and (d) CuZn36 (C27450) lead-free brasses. White dots in (a) represent Pb particles in the  $\alpha/\beta$  interfaces. The  $\beta$ -phase is located in the recess areas, as a result of its higher dissolution during chemical etching.

### 3.2. Machinability Evaluation

During the machinability evaluation, two quality characteristics were selected: the cutting force (CF) and the surface roughness (SR). For reliability reasons, the experiments for the two quality characteristics were repeated twice; see experimental results in Table 5 (“REP” stands for replicate). The particular quality characteristics, namely cutting force (CF) and surface roughness (SR), have to be minimized and hence the “smaller-the-better” type quality criterion has been selected for each of the data means and signal-to-noise responses. The governing Equation (1) for the signal-to-noise ratio (S/N) using the above criterion was:

$$S/N = -10 \log\left(\frac{\sum y_i^2}{n}\right), \quad (1)$$

where  $y_i$  corresponds to the performance value of the  $i$ th experiment and  $n$  was the number of repetitions.

**Table 5.** Experimental results for cutting force (CF) and surface roughness (SR).

Number of Experiment	Material	Quality Characteristics Results					
		CF (N) REP 1	CF (N) REP 2	CF (N) AVERAGE	SR ( $\mu\text{m}$ ) REP 1	SR ( $\mu\text{m}$ ) REP 2	SR ( $\mu\text{m}$ ) AVERAGE
1	CW510L	81	80	81	1.8	1.7	1.8
2	CW511L	214	223	219	2.1	2.2	2.1
3	C27450	344	348	346	2.9	2.7	2.8
4	CW614N	454	454	454	10.8	11.4	11.1
5	C27450	91	90	91	1.9	2.0	2.0
6	CW614N	86	87	87	2.1	2.2	2.2
7	CW510L	544	535	540	8.1	8.0	8.0
8	CW511L	441	450	446	2.2	2.5	2.3
9	CW614N	63	61	62	2.6	2.3	2.4
10	C27450	301	299	300	5.7	5.6	5.6
11	CW511L	202	215	209	1.8	1.8	1.8
12	CW510L	328	324	326	5.6	5.1	5.4
13	CW511L	122	129	126	4.4	4.3	4.3
14	CW510L	181	174	178	3.3	4.5	3.9
15	CW614N	131	131	131	2.1	2.1	2.1
16	C27450	242	245	244	4.7	5.8	5.3

### 3.3. Cutting-Force Optimization

Characteristic histograms of cutting force, produced under various turning conditions, are shown in Figure 6.

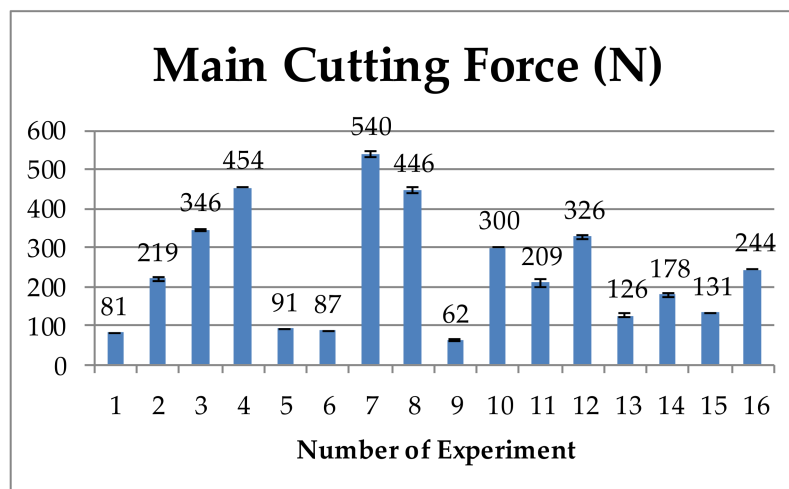


**Figure 6.** Histogram showing the main cutting force (N) that resulted under various turning conditions.

The plots of main effects of S/N ratios (Figure 7) and data means (Figure 8) indicated that the optimum values of cutting parameters that minimize the cutting force were the following:

1. Alloy type: CW614N;
2. Cutting speed: 2250 rpm;
3. Depth of cut: 0.5 mm;
4. Feed rate: 150 mm/min.

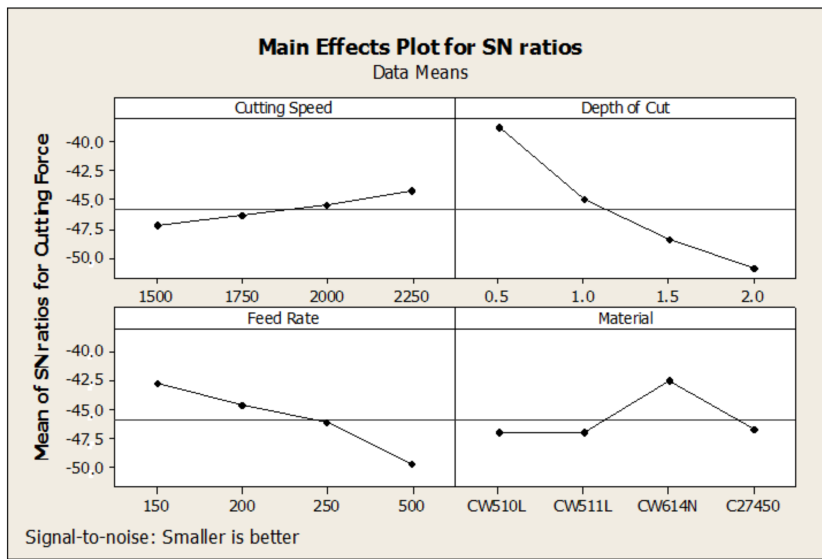


**Figure 7.** Diagrams showing the variation of signal-to-noise (S/N) ratios for cutting force as a function of the cutting parameters (cutting speed, depth of cut, feed rate and material).

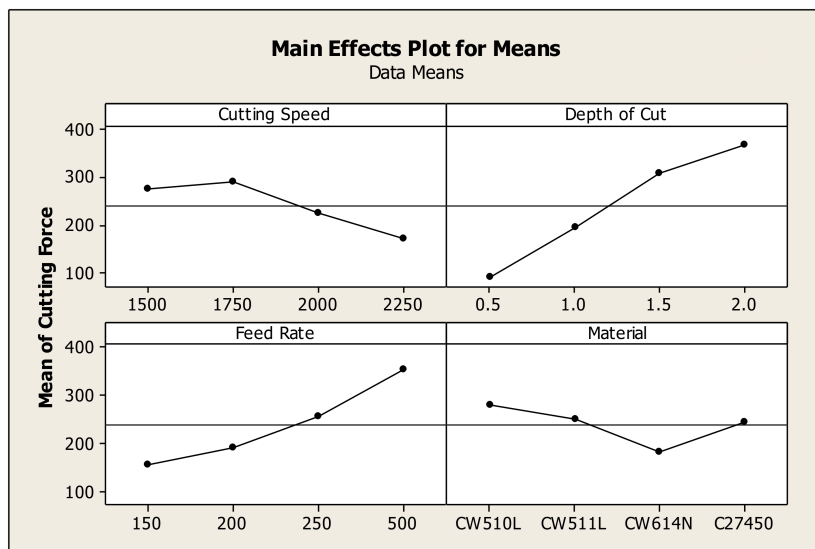


**Figure 8.** Diagrams showing the data means for cutting force as a function of the cutting parameters (cutting speed, depth of cut, feed rate and material).

Experimental results indicated that the most critical factor affecting the cutting force (CF), during brass-bar machining, is the depth of cut, while the less influential factors for CF are the cutting speed and the type of brass alloy (Table 6). An important step in the Taguchi methodology is to perform confirmation experiments. The predicted S/N ratio using the optimal level of the design parameters can be calculated by the following equation [37]:

$$(S/N)_{\text{predicted}} = (S/N)_m + \sum_{i=1}^n ((S/N)_i - (S/N)_m), \tag{2}$$

where  $(S/N)_m$  is the total mean S/N ratio,  $(S/N)_i$  is the S/N ratio at the optimal level of the  $i$ th parameter, and  $n$  is the number of the main design parameters that affect the quality characteristic.

In the case of cutting force:  $(S/N)_m = -45.8369$ .

So, the predicted S/N ratio using the optimal parameters for cutting force (CF) is given below:

$$(S/N)_{\text{predicted}} = -30.78$$

From Equation (1) and substituting the (S/N) term with the predicted value (−30.78) this yields to:

$$y = \text{Predicted Cutting Force} = 34.59 \text{ N}$$

**Table 6.** Response table for signal-to-noise (S/N) ratios for cutting force.

Response Table	Cutting Speed (rpm)	Depth of Cut (mm)	Feed Rate (mm/min)	Material
Level 1	−47.21	−38.77	−42.74	−47.00
Level 2	−46.37	−45.01	−44.63	−47.03
Level 3	−45.51	−48.54	−46.15	−42.52
Level 4	−44.26	−51.03	−49.82	−46.80
Difference	2.95	12.26	7.08	4.51
Rank	4	1	2	3

Table 7 shows the comparison of the estimated (predicted) and the measured (experimental) cutting force values using the optimal conditions, where it has been deduced that there is sufficient agreement between the predicted (34.59 N) and the experimental cutting force (39.37 N) values.

**Table 7.** Results of confirmation experiment.

Quality Characteristic	Cutting Speed (rpm)	Depth of Cut (mm)	Feed Rate (mm/min)	Material	Experimental Value	Predicted Value
Cutting Force	2250	0.5	150	CW614N	39.37 N	34.59 N
Surface Roughness	1750	0.5	150	CW511L	1.71 $\mu\text{m}$	1.22 $\mu\text{m}$

In terms of cutting force, it seems that the conventional leaded alloy CW614N exhibits the highest machinability performance, signifying the dominant effect of the presence of Pb on cutting force reduction, as was also confirmed in case of chip breakability [8].

#### 3.4. Surface-Roughness Optimization

Characteristic histogram of surface roughness, produced under various turning conditions, is shown in Figure 9.

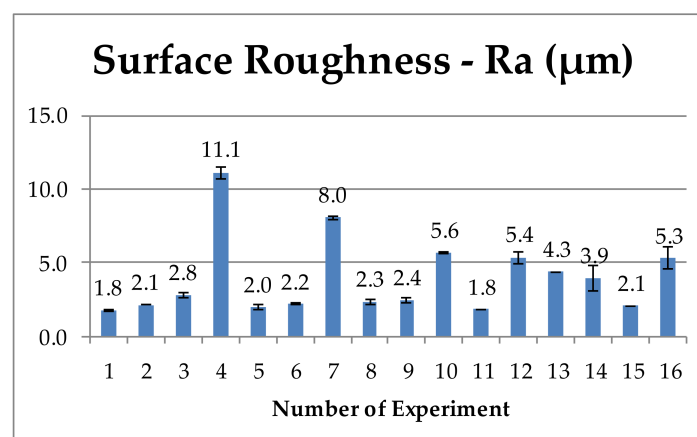


**Figure 9.** Histogram showing the surface roughness—Ra ( $\mu\text{m}$ ) resulting under various turning conditions.

The graphs of the responses of S/N ratios (Figure 10) and data means (Figure 11) indicated that the values of cutting parameters which optimize the surface roughness were the following:

1. Alloy type: CW511L;
2. Cutting speed: 1750 rpm;
3. Depth cut: 0.50 mm;
4. Feed rate: 150 mm/min.

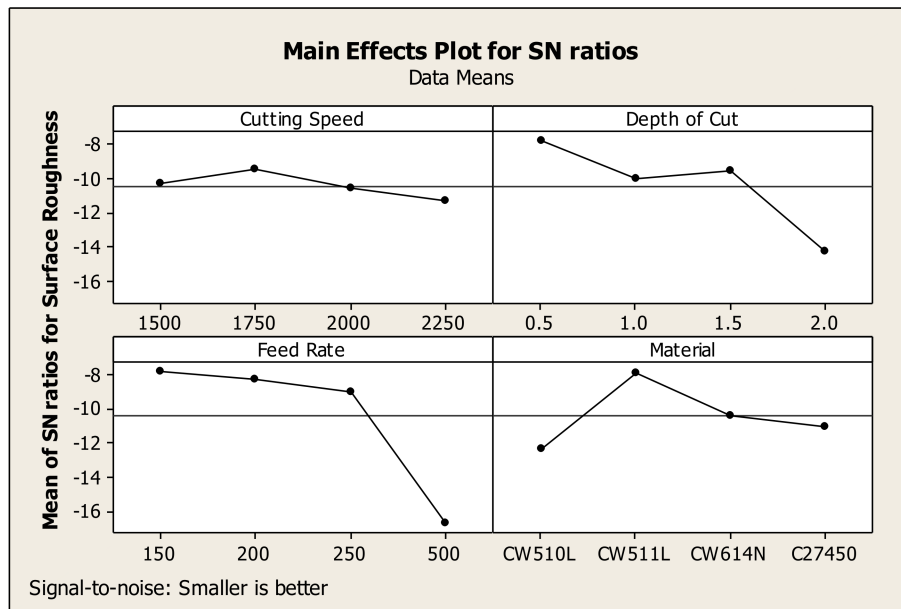


Figure 10. Diagrams showing the variation of S/N ratios for surface roughness as a function of the cutting parameters (cutting speed, depth of cut, feed rate and material).

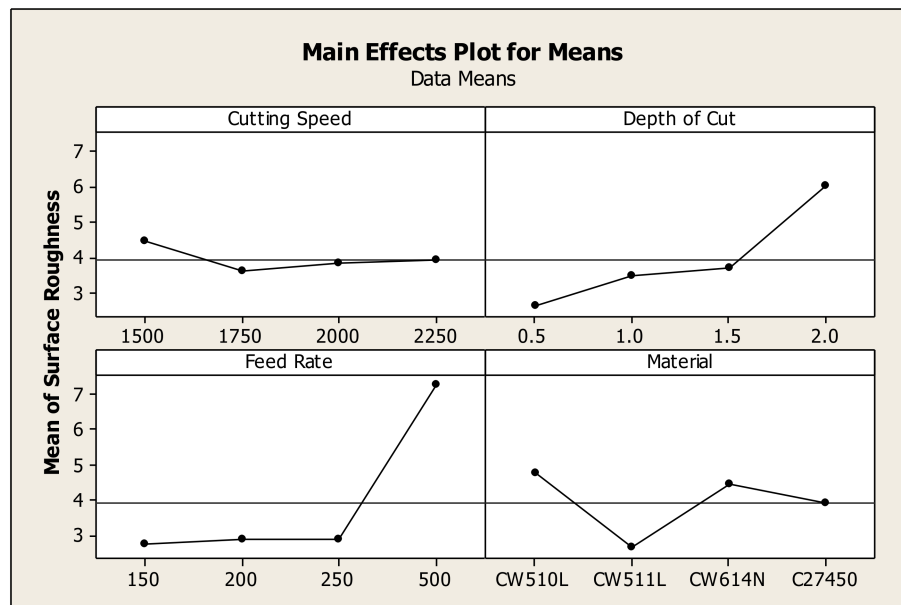


Figure 11. Diagrams showing the data means for surface roughness as a function of the cutting parameters (cutting speed, depth of cut, feed rate and material).

Experimental results indicated that the most critical factor affecting the surface roughness (SR), during brass-bar machining, is the feed rate, while SR seems to be not so highly sensitive to cutting

speed and the type of brass alloy used varied (Table 8). In order to verify the adequacy of the Taguchi methodology, a confirmation test was performed. The predicted S/N ratio using the optimal level of the design parameters can be calculated by Equation (2).

**Table 8.** Response table for S/N ratios for surface roughness.

Response Table	Cutting Speed (rpm)	Depth of Cut (mm)	Feed Rate (mm/min)	Material
Level 1	−10.325	−7.819	−7.776	−12.368
Level 2	−9.496	−10.034	−8.315	−7.957
Level 3	−10.623	−9.603	−8.983	−10.396
Level 4	−11.331	−14.318	−16.700	−11.054
Difference	1.836	6.499	8.924	4.411
Rank	4	2	1	3

In the case of surface roughness:

$$(S/N)_m = -10.4436$$

So, the predicted S/N ratio using the optimal parameters for surface roughness (SR) can be obtained and calculated as previously:

$$(S/N)_{\text{predicted}} = -1.72$$

Therefore, the predicted surface roughness, as calculated by Equation (1), is:

$$y = \text{Predicted Surface Roughness} = 1.22 \mu\text{m}$$

Table 7 shows the comparison of the estimated (predicted) and the measured (experimental) surface roughness where it seems that there is a relative agreement between the predicted (1.22  $\mu\text{m}$ ) and the experimental (1.71  $\mu\text{m}$ ) surface-roughness values.

Regarding surface roughness, the highest score was achieved by lead-free alloy CW511L, compared with the other lead-free alloys studied and a typical leaded one, which pinpoints a promising candidate whereby surface quality is considered as the most critical machinability criterion.

### 3.5. Analysis of Variance (ANOVA)

The contribution of each factor to the cutting force and surface roughness during the machining of lead-free brass alloys can be determined by performing ANOVA based on equations [37–39], which are listed below:

$$SS_T = \sum_i^m n_i^2 - \frac{1}{m} \left( \sum_{i=1}^m n_i \right)^2, \text{ Total Sum of Squares } (SS_T) \quad (3)$$

$$SS_p = \sum_{j=1}^t \frac{(S_{nj})^2}{t} - \frac{1}{m} \left( \sum_{i=1}^m n_i \right)^2, \text{ Factorial Sum of Squares } (SS_p) \quad (4)$$

$$V_p(\%) = \frac{SS_p}{D_p} \times 100\%, \text{ Factorial Variance } (V_p) \quad (5)$$

$$SS'_p = SS_p - D_p V_e, \text{ Corrected Sum of Squares of a factor } (SS'_p) \quad (6)$$

$$P_p(\%) = \frac{SS'_p}{SS_T} \times 100\%, \text{ Percent Contribution } (P_p) \quad (7)$$

where  $m$  is the total number of the experiments,  $n_i$  is the S/N ratio at the  $i$ th test,  $S_{nj}$  the sum of the S/N ratio involving this factor and level  $j$ ,  $D_p$  is the degree of freedom for each factor, and  $V_e$  is the error variance.

The percent contribution ( $P_p$ ) is used to evaluate the significance of the factorial change on the quality characteristic, i.e., cutting force and surface roughness [40]. The results of ANOVA for the cutting force and surface roughness are summarized in Tables 9 and 10. The data given in Tables 9 and 10 show the contribution of the four factors, i.e., cutting speed, depth of cut, feed rate and materials to the quality characteristics. It is clear that, among the selected factors, the depth of cut and feed rate have the major influence on the cutting force and surface roughness, respectively. By ranking their relative contributions, the sequence of the four factors affecting the cutting force is the depth of cut, the feed rate, the material type and, finally, the cutting speed, while for surface roughness the corresponding sequence in decreasing order is the following: feed rate, depth of cut, material type and, finally, cutting speed. In the ANOVA analysis, the percentage error ( $P_e$ ) contribution to the total variance is lower than 15% (0.43% and 10.51% for cutting force and surface roughness, respectively), showing that no important factor is missing in the experimental design [37].

**Table 9.** Analysis of variance (ANOVA) for the cutting force.

Factor	Degrees of Freedom	Sum of Squares (SS)	Corrected Sum of Squares (SS')	Variance	Percent Contribution $P_p$ (%)	Rank
Cutting Speed	3	19.0425	18.8254	6.3475	3.5728	4
Depth of Cut	3	339.5408	339.3238	113.1803	64.3992	1
Feed Rate	3	108.0831	107.8660	36.0277	20.4715	2
Material	3	58.8660	58.6489	19.6220	11.1308	3
Error	19	1.3746	2.2428	0.0723	0.4257	-
Total	31	526.9070	526.9070	-	100.0000	-

**Table 10.** Analysis of variance (ANOVA) for the surface roughness.

Factor	Degrees of Freedom	Sum of Squares (SS)	Corrected Sum of Squares (SS')	Variance	Percent Contribution $P_p$ (%)	Rank
Cutting Speed	3	7.3498	3.5422	2.4499	0.9460	4
Depth of Cut	3	91.6606	87.8530	30.5535	23.4625	2
Feed Rate	3	210.9051	207.0974	70.3017	55.3085	1
Material	3	40.4101	36.6025	13.4700	9.7753	3
Error	19	24.1149	39.3453	1.2692	10.5078	-
Total	31	374.4404	374.4404	-	100.0000	-

#### 4. Conclusions

The continuously increasing strictness of regulations governing drinking-water quality parameters has required explicitly the design and use of new and environmentally friendly alloys for the fabrication of components in use in domestic water circuits. Copper alloys (brasses) are principally used for the manufacturing of fittings, valves and connectors for such applications. In this framework, the present study was focused on machinability research using optimization techniques for lead-free brass alloys which are destined to replace conventional leaded brasses for the fabrication of complex-shaped components. The findings of the current research are summarized below.

The optimization, of the two additional machinability criteria, i.e., cutting force and surface roughness, was attempted using DOE and ANOVA approaches for the selected lead-free brass alloys (CW510L, CW511L and C27450) compared with a reference leaded alloy (CW614N). The main findings of this investigation are the following:

- a. Cutting force is optimized using the following conditions (using signal-to-noise and data means): the optimal alloy type is CW614N, cutting speed = 2250 rpm, depth cut = 0.5 mm and feed rate = 150 mm/min. ANOVA showed that the contributions of the above factors are 11.13%, 3.57%, 64.40% and 20.47%, respectively. The analysis coming from data means and S/N response tables indicated that the depth of cut is the most influential factor, while ANOVA proved that this parameter has the highest percent contribution ( $P_p = 64.40\%$ ) and, consequently, plays the most affecting role in the determination of cutting-force measurements. Also, since the percentage

- error (0.43%) contribution in ANOVA analysis is lower than 50%, no repetition of any experiment is needed.
- b. Surface roughness is optimized using the following conditions (using signal-to-noise and data means): the optimal alloy type is CW511L, cutting speed = 1750 rpm, depth cut = 0.50 mm and feed rate = 150 mm/min. The contributions of the above factors are 9.78%, 0.95%, 23.46% and 55.31%, respectively, according to the ANOVA technique. The same ranking order was also achieved by the S/N method. Feed rate has the highest percentage contribution ( $P_p = 55.31\%$ ), as it was proven by ANOVA and it constitutes also the most influential factor according to data means and S/N response tables. Since the percentage error (10.51%) contribution deduced from ANOVA analysis is lower than 50%, no experimental repetition is required.
  - c. Confirmation experiments indicated that a considerable agreement leading to around 10% deviation was achieved for cutting force (predicted 34.59 N vs. experimental 39.37 N). Although surface-roughness experiments resulted in higher differences (predicted 1.22  $\mu\text{m}$  vs. experimental 1.71  $\mu\text{m}$ ), the obtained values are considered comparable and of the same order of magnitude, taking into account the entire spectrum of the tested conditions.
  - d. In terms of cutting-force optimization, the leaded alloy CW614N exhibited the highest machinability performance, while for surface roughness, the lead-free CW511L was appointed as the optimum alloy selection. Although leaded brasses still dominate in the machining industry, this result offers a hopeful perspective, expanding the horizons for further research towards machinability improvement through further alloy and microstructural design.

## 5. Further Research

This study was a part of an extended industrial research project mostly dedicated to delineating the properties and machinability of eco-friendly brass alloys compared with a common machinable brass widely used in industry. The next steps have also been planned in order to pursue a modification of microstructure using thermal-processing routes without changing the standard alloy composition, and aiming to achieve and/or exceed high machinability standards. This innovative work is in progress and the prospective results are going to be completed and disseminated in a future work shortly.

**Acknowledgments:** The authors wish to express special thanks to the Administration and Quality Division of FITCO S.A. for continuous support and providing samples for the current investigation. Special thanks are also addressed to A. Rikos and A. Vazdirvanidis (ELKEME S.A.), for their assistance in metallographic sample preparation and examination and for the constructive technical discussion.

**Author Contributions:** All authors contributed to the implementation of this scientific research work.

**Conflicts of Interest:** The authors declare no conflict of interest.

## References

1. Kim, H.S.; Kim, W.Y.; Song, K.H. Effect of post-heat treatment in ECAP processed Cu-40%Zn brass. *J. Alloys Compd.* **2012**, *536*, S200–S203. [[CrossRef](#)]
2. Kumar, R.; Dasharath, S.M.; Kang, P.C.; Koch, C.C.; Mula, S. Enhancement of mechanical properties of low stacking fault energy brass processed by cryorolling followed by short-annealing. *Mater. Des.* **2015**, *67*, 637–643. [[CrossRef](#)]
3. Pantazopoulos, G.; Toulfatzis, A. Fracture modes and mechanical characteristics of machinable brass rods. *Metallogr. Microstruct. Anal.* **2012**, *1*, 106–114. [[CrossRef](#)]
4. Li, S.; Kondoh, K.; Imai, H.; Atsumi, H. Fabrication and properties of lead-free machinable brass with Ti additive by powder metallurgy. *Powder Technol.* **2011**, *205*, 242–249. [[CrossRef](#)]
5. La Fontaine, A.; Keast, V.J. Compositional distributions in classical and lead-free brasses. *Mater. Charact.* **2006**, *57*, 424–429. [[CrossRef](#)]
6. Toulfatzis, A.; Pantazopoulos, G.; Paipetis, A. Fracture behavior and characterization of lead-free brass alloys for machining applications. *J. Mater. Eng. Perform.* **2014**, *23*, 3193–3206. [[CrossRef](#)]

7. Pantazopoulos, G. Leaded brass rods C38500 for automatic machining operations. *J. Mater. Eng. Perform.* **2002**, *11*, 402–407. [[CrossRef](#)]
8. Toulfatzis, A.I.; Pantazopoulos, G.A.; Besseris, G.J.; Paipetis, A.S. Machinability evaluation and screening of leaded and lead-free brasses using a non-linear robust multifactorial profiler. *Int. J. Adv. Manuf. Technol.* **2016**, *86*, 3241–3254. [[CrossRef](#)]
9. Doostmohammadi, H.; Moridshahi, H. Effect of Si on microstructure, ordering transformation and properties of the Cu<sub>60</sub>Zn<sub>40</sub> alloy. *J. Alloys Compd.* **2015**, *640*, 401–407. [[CrossRef](#)]
10. Rajabi, Z.; Doostmohammadi, H. Effect of addition of tin on the microstructure and machinability of  $\alpha$ -brass. *Mater. Sci. Technol.* **2018**. [[CrossRef](#)]
11. Imai, H.; Shufeng, L.; Atsumi, H.; Kosaka, Y.; Kojima, A.; Kondoh, K. Development of lead-free machinable brass with bismuth and graphite particles by powder metallurgy process. *Mater. Trans.* **2010**, *51*, 855–859. [[CrossRef](#)]
12. Suksongkarm, P.; Rojananan, S.; Rojananan, S. Using recycled bismuth-tin solder in novel machinable lead-free brass. *Mater. Trans.* **2017**, *58*, 1754–1760. [[CrossRef](#)]
13. Nobel, C.; Hofmann, U.; Klocke, F.; Veselovac, D. Experimental investigation of chip formation, flow, and breakage in free orthogonal cutting of copper-zinc alloys. *Int. J. Adv. Manuf. Technol.* **2016**, *84*, 1127–1140. [[CrossRef](#)]
14. Toulfatzis, A.; Pantazopoulos, G.; Paipetis, A. Microstructure and properties of lead-free brasses using post-processing heat treatment cycles. *Mater. Sci. Technol.* **2016**, *32*, 1771–1781. [[CrossRef](#)]
15. Klocke, F.; Nobel, C.; Veselovac, D. Influence of tool coating, tool material, and cutting speed on the machinability of low-leaded brass alloys in turning. *Mater. Manuf. Process.* **2016**, *31*, 895–1903. [[CrossRef](#)]
16. Schultheiss, F.; Johansson, D.; Bushlya, V.; Zhou, J.; Nilsson, K.; Ståhl, J.E. Comparative Study on the Machinability of Lead-Free Brass. *J. Clean. Prod.* **2017**, *149*, 366–377. [[CrossRef](#)]
17. Ekinovic, S.; Begovic, E.; Silajdzija, A. Comparison of machined surface quality obtained by high-speed machining and conventional turning. *Mach. Sci. Technol.* **2007**, *11*, 531–551. [[CrossRef](#)]
18. Huo, D.; Chen, W.; Teng, X.; Lin, C.; Yang, K. Modeling the influence of tool deflection on cutting force and surface generation in micro-milling. *Micromachines* **2017**, *8*, 188. [[CrossRef](#)]
19. Jomaa, W.; Songmene, V.; Bocher, P. Predictive analytical modeling of cutting forces generated by high-speed machining of ductile and hard metals. *Mach. Sci. Technol.* **2017**, *21*, 335–361. [[CrossRef](#)]
20. Toulfatzis, A.; Besseris, G.; Pantazopoulos, G.; Stergiou, C. Characterization and comparative machinability investigation of extruded and drawn copper alloys using non-parametric multi-response optimization and orthogonal arrays. *Int. J. Adv. Manuf. Technol.* **2011**, *57*, 811–826. [[CrossRef](#)]
21. Hassan, K.; Kumar, A.; Garg, M.P. Experimental investigation of material removal rate in CNC turning using Taguchi method. *Int. J. Eng. Res. Appl.* **2012**, *2*, 1581–1590.
22. Vaxevanidis, N.M.; Kechagias, J.D.; Fountas, N.A.; Manolakos, D.E. Evaluation of machinability in turning of engineering alloys by applying artificial neural networks. *Open Constr. Build. Technol. J.* **2014**, *8*, 389–399. [[CrossRef](#)]
23. Gaitonde, V.N.; Karnik, S.R.; Davim, J.P. Optimal MQL and cutting conditions determination for desired surface roughness in turning of brass using genetic algorithms. *Mach. Sci. Technol.* **2012**, *16*, 304–320. [[CrossRef](#)]
24. Kilickap, E.; Yardimeden, A.; Çelik, Y.H. Mathematical modelling and optimization of cutting force, tool wear and surface roughness by using artificial neural network and response surface methodology in milling of Ti-6242S. *Appl. Sci.* **2017**, *7*, 1064. [[CrossRef](#)]
25. Koklu, U.; Basmaci, G. Evaluation of tool path strategy and cooling condition effects on the cutting force and surface quality in micromilling operations. *Metals* **2017**, *7*, 426. [[CrossRef](#)]
26. Haddag, B.; Atlati, S.; Nouari, M.; Moufki, A. Dry machining aeronautical aluminum alloy AA2024-T351: Analysis of cutting forces, chip segmentation and built-up edge formation. *Metals* **2016**, *6*, 197. [[CrossRef](#)]
27. Ahmed, Y.S.; Youssef, H.; El-Hofy, H.; Ahmed, M. Prediction and optimization of drilling parameters in drilling of AISI 304 and AISI 2205 steels with PVD monolayer and multilayer coated drills. *J. Manuf. Mater. Process.* **2018**, *2*, 16. [[CrossRef](#)]
28. Box, G.E.P.; Hunter, W.G.; Hunter, J.S. *Statistics for Experimenters: Design, Innovation, Discover*, 2nd ed.; Wiley: Hoboken, NJ, USA, 2005.
29. Taguchi, G. *Introduction to Quality Engineering*; Asian Productivity Organization: Tokyo, Japan, 1986.

30. European Committee for Standardization (CEN). *BS EN 12164: Copper and Copper Alloys: Rod for Free Machining Purposes*; European Committee for Standardization (CEN): Brussels, Belgium, 2011.
31. American Society for Testing and Materials (ASTM). *ASTM E407-07ε1: Standard Practice for Microetching Metals and Alloys*; American Society for Testing and Materials (ASTM): West Conshohocken, PA, USA, 2007.
32. CEN. *BS EN ISO 6892-1: Metallic Materials—Tensile Testing—Part 1: Method of Test at Room Temperature*; European Committee for Standardization (CEN): Brussels, Belgium, 2009.
33. International Organization for Standardization (ISO). *ISO 6507-1: Metallic Materials—Vickers Hardness Test—Part 1: Test Method*; International Organization for Standardization (ISO): Geneva, Switzerland, 2005.
34. ISO. *ISO 3685: Tool-Life Testing with Single-Point Turning Tools*; International Organization for Standardization (ISO): Geneva, Switzerland, 1993.
35. ASME. *ANSI B46.1: Surface Texture (Surface Roughness, Waviness, and Lay)*; ASME: New York, NY, USA, 2009.
36. Pantazopoulos, G.; Vazdirvanidis, A. Characterization of microstructural aspects of machinable  $\alpha$ - $\beta$  phase brass. *Microsc. Anal.* **2008**, *22*, 13–16.
37. Yousefieh, M.; Shamanian, M.; Arghavan, A.R. Analysis of design of experiments methodology for optimization of pulsed current GTAW process parameters for ultimate tensile strength of UNS S32760 welds. *Metallogr. Microstruct. Anal.* **2012**, *1*, 85–91. [[CrossRef](#)]
38. Ma, Y.; Hu, H.; Northwood, D.; Nie, X. Optimization of the electrolytic plasma oxidation processes for corrosion protection of magnesium alloy AM50 using the Taguchi method. *J. Mater. Process. Technol.* **2007**, *182*, 58–64. [[CrossRef](#)]
39. Yousefieh, M.; Shamanian, M.; Saatchi, A. Optimization of the pulsed current gas tungsten arc welding (PCGTAW) parameters for corrosion resistance of super duplex stainless steel (UNS S32760) welds using the Taguchi method. *J. Alloys Compd.* **2011**, *509*, 782–788. [[CrossRef](#)]
40. Mariajayaprakash, A.; Senthilvelan, T. Optimizing process parameters of screw conveyor (sugar mill boiler) through failure mode and effect analysis (FMEA) and Taguchi method. *J. Fail. Anal. Prev.* **2014**, *14*, 772–783. [[CrossRef](#)]



© 2018 by the authors. Licensee MDPI, Basel, Switzerland. This article is an open access article distributed under the terms and conditions of the Creative Commons Attribution (CC BY) license (<http://creativecommons.org/licenses/by/4.0/>).